Spatial patterns of disconnectivity explain catchment-scale sediment dynamics and transfer efficiencies

Authors: Mike Turley[1*], Marwan A. Hassan[1]

[1] Department of Geography, The University of British Columbia, Vancouver, B.C., Canada.

*Corresponding author: Mike Turley (mbturley@student.ubc.ca)

Key Points:

- Disconnectivity is the dominant but inefficient state of a system in transferring matter and energy within and between system components
- Sources of disconnectivity were found to accurately explain catchment-scale sediment dynamics
- During extreme events, the efficiency of sediment transfer increases resulting in rapid adjustment

Abstract

While connectivity studies are becoming common in the Earth sciences, disconnectivity has received much less attention. Sediment storage is the direct result of sediment disconnectivity and can provide concrete evidence of the spatial patterns of disconnectivity at the catchment-scale. In this study we explore the catchment-scale sediment dynamics of the Tahoma Creek watershed, a high-gradient glacio-volcanic landscape, within a sediment budget framework and identify and map sources of disconnectivity to determine if they explain the spatial patterns and estimated efficiencies of sediment transfers. We found that up to 80% of the total eroded sediment is sourced from the proglacial zone. The proglacial zone is characterized by high connectivity resulting from frequent debris flows and floods, and rapidly responds to changing conditions. Down valley however, sources of disconnectivity become increasingly more prevalent, the hillslopes become decoupled from the channel, and a majority of the eroded sediment is redeposited with as little as ~15% reaching the outlet. The spatial distribution of sources of disconnectivity and their upslope affected areas explains, to a large degree, catchment-scale sediment dynamics and sediment transfer efficiencies and is in close agreement with quantitative connectivity estimates. We find that steep, glaciated watersheds are predominantly disconnected over human timescales and suggest that disconnectivity is the dominant state of landscapes over most timescales of interest. Mapping sources of disconnectivity provides a straightforward and concrete approach to estimating system disconnectivity and can increase confidence when paired with quantitative indices.

Plain Language Summary

Mountain watersheds supply freshwater and sediment to downstream river systems, affecting flooding, fish habitat, and water quality. We argue that understanding the spatial and temporal patterns of sediment movement within a landscape requires knowing where and for how long sediment is stored, and the overall efficiency of sediment transfer between different parts of the landscape. We illustrate the importance and utility of mapping landforms and landscape characteristics that delay or disrupt sediment movement using the Tahoma Creek watershed as an example. This watershed drains a portion of Mount Rainier, a volcano shaped by glaciers in Washington, USA, and is incredibly dynamic. We find that landforms and landscape characteristics that limit sediment movement are common, and that mapping them gives an accurate picture of sediment movement patterns. Glaciers dramatically reshape the landscape, which controls sediment supply and movement patterns, and their legacy remains for thousands of years after they retreat. We also make use of high-resolution elevation data representing the land surface in 2002, 2008, and 2012 to quantify how much erosion, transport, and deposition occurred and how efficiently sediment was transported. We find that sediment is transported more efficiently during extreme events, such as the 2006 floods.

1 Introduction

Mountain watersheds supply freshwater and sediment to downstream river systems, affecting flooding, fish habitat, and water quality. The movement of water and sediment within a landscape is dependent on coupling between upstream sediment sources and downstream river

systems, and more generally, landscape connectivity. While connectivity is becoming an increasingly popular topic of study (Slaymaker & Embleton-Hamann, 2018; Najafi et al., 2021), investigations that explicitly consider disconnectivity remain relatively uncommon (some key exceptions include: Walling, 1983; Hooke, 2003; Fryirs et al. 2007a, 2007b; Fryirs, 2013; Hoffmann, 2015; Grant et al., 2017).

Within the literature, the infrequent and spatially limited nature of mass and energy transfer within systems is often noted (e.g., Hoffmann, 2015; Repasch et al., 2020; Ben-Israel et al., 2022), suggesting that disconnectivity is the more common state of geomorphic systems (an idea explored further in this paper). We define disconnectivity as the dominant but inefficient state of a system in transferring matter and energy within and between system components. This definition modifies previous definitions (Chorley & Kennedy, 1971; Wohl et al., 2019), with additional emphasis on the fragmented and inefficient nature of most landscapes.

Disconnectivity occurs as a result of landforms (Fryirs et al., 2007a), bio-geomorphic characteristics of the system (i.e., vegetation [e.g., Cienciala, 2021], topography [e.g., Cavalli et al., 2013], network structure [e.g., Cossart & Fressard, 2017; Gran & Czuba, 2017], etc.), negative process-form feedbacks (Cossart, 2008; Lane et al., 2017), thresholds (Schumm, 1979), and process discontinuity (Grant et al., 2017) that reduce the efficiency of sediment transfer through storage. A consideration of disconnectivity is required to explain sediment storage patterns and landscape morphology (Hoffmann, 2015), interpret sedimentary archives, explain buffering of climatic or tectonic signals and system response times (Tofelde et al., 2021; Ben-Israel et al., 2022), and explain landscape resilience (Fryirs, 2017; Lisenby et al., 2020). Disconnectivity is also required to explain how and why landscapes can be in a state of disequilibrium with current processes and conditions, a fundamental consideration for previously glaciated landscapes (Church & Ryder, 1972; Ballantyne, 2002). Additionally, the effective timescales of landforms and characteristics that cause or increase disconnectivity (discussed later in this paper) may not always match the timescales over which connectivity operates. For these reasons, we believe the explicit consideration of disconnectivity is often warranted. Connectivity on the other hand, may be defined as the spatially and temporally limited efficient state of a system in transferring matter and energy within and between system components. Wohl et al. (2019) provides a useful review of the subject, including what we (field of geomorphology) do and don’t yet know.

Many mountainous landscapes have been repeatedly reshaped and reorganized by glacial cycles throughout the Quaternary Period. Glacial retreat since the Last Glacial Maximum has resulted in non-glacial processes operating on relict glacial topography and process-form disequilibrium, so that topographic signatures don't match contemporary geomorphic process domains (Brardinoni & Hassan, 2006). As a result, glacial and postglacial landscapes alike are dynamic, complex, and heterogeneous systems shaped by a variety of processes. Remnant glacial deposits are often thick and unconsolidated, making them important sources of sediment when accessible. In British Columbia, a positive relation was found between specific suspended sediment and drainage area for basins up to 30,000 km^2 due to secondary reworking of glacial sediments (Church & Slaymaker, 1989). Glaciofluvial terraces, for example, have been identified as important sources of sediment in postglacial basins (Reid et al., 2021; Scott & Collins, 2021). While research in postglacial systems has primarily focused on aspects of paraglacial sedimentation (Church & Ryder, 1972), few studies have explored the degree to which glacial landscapes are uniquely and highly fragmented (examples include Brardinoni & Hassan, 2006; Hoffmann et al., 2013).

It is also important to note that while the term disconnectivity became prevalent only recently, the concept has been inferred for a long time when calculating sediment budgets (Dietrich et al., 1982). A sediment budget is a quantitative description of the rates of production, transport, and export of sediment that incorporates changes in storage, and specifies the contribution from different processes (Dietrich et al., 1982; Reid & Dunne, 1996; Hinderer, 2012; Reid & Dunne, 2016). In conceptualizing the system as a sediment cascade through temporary sediment stores, sediment budgets can reconcile the contemporaneously continuous and discontinuous processes that operate over different timescales (Grant et al., 2017) and therefore facilitate studies of disconnectivity.

Fryirs et al. (2007a) presents a useful categorization system of sources of disconnectivity. In this system, sources of disconnectivity are classified as buffers, barriers or blankets based on whether they prevent sediment from entering the channel (lateral disconnectivity), disrupt sediment moving along the channel (longitudinal disconnectivity), or prevent vertical reworking of sediment through smothering (vertical disconnectivity), respectively (Fryirs et al., 2007a, 2007b; Fryirs, 2013). Disconnectivity is a key property of the system. A given landscape's tectonic and climatic history results in unique valley geometry, spatial organization of landform assemblages, and topographic complexity, which controls the spatial patterns of hillslope-channel coupling

and sediment disconnectivity (Hassan et al., 2018). Disconnectivity in turn controls the location and volume of sediment inputs to the channel and subsequently channel morphology, channel geometry, and bed texture (Hassan et al., 2018, Reid et al., 2021). Channel characteristics determine the functioning of the fluvial system including channel stability and migration (Eaton et al., 2020), flooding and its' geomorphic effectiveness (Al-Ghorani et al., 2022), and aquatic ecosystems (e.g., Cienciala and Hassan, 2013). An understanding of disconnectivity is then required to interpret the system at different scales, both temporal (e.g., geomorphic effectiveness of floods relating to tectonic and glacial cycles), and spatial (e.g., channel bed texture relating to valley geometry). However, the utility of disconnectivity has not been fully explored.

This paper aims to illustrate the link between contemporary processes operating on a mountainous landscape shaped by glaciations, the location, types, and relative abundance of sources of disconnectivity, and the resulting spatial patterns of sediment dynamics and transfer efficiencies. In particular we (i) explore the catchment-scale sediment dynamics of a high-gradient glacio-volcanic landscape within a sediment budget framework utilizing multitemporal high-resolution DEMs and fieldwork data, and (ii) identify and map sources of disconnectivity to determine if they explain the spatial patterns and estimated efficiencies of sediment transfers. We present general descriptions of sources of disconnectivity that might be found in similar high-mountain, glaciated watersheds and discuss the utility of using them to gain understanding of sediment dynamics. The Tahoma Creek watershed is spatially heterogeneous and dynamic, making it an ideal location to illustrate sources of disconnectivity. Additionally, the spatial patterns of sources of disconnectivity are compared to previously published quantitative estimations of connectivity in this basin (Turley et al., 2021).

2 Study Site

The Tahoma Creek Watershed drains approximately 40 km^2 of the southwest flank of what is traditionally named təqʷuʔmaʔ (later named Mount Rainier by white settlers), an active stratovolcano within the Cascade Range of Washington, USA, in the territory of the dxʷsqʷali? abš (Nisqually) and spuyaləpabš (Puyallup) tribes (Figure 1). Tahoma Creek emanates from and follows the last glacial maximum (LGM) path carved by the South Tahoma Glacier for ~14 km. Distances are measured along the river's centerline beginning at the 2019 glacier terminus, denoted in "river kilometers – RKM". The river flows through several distinct zones along its'

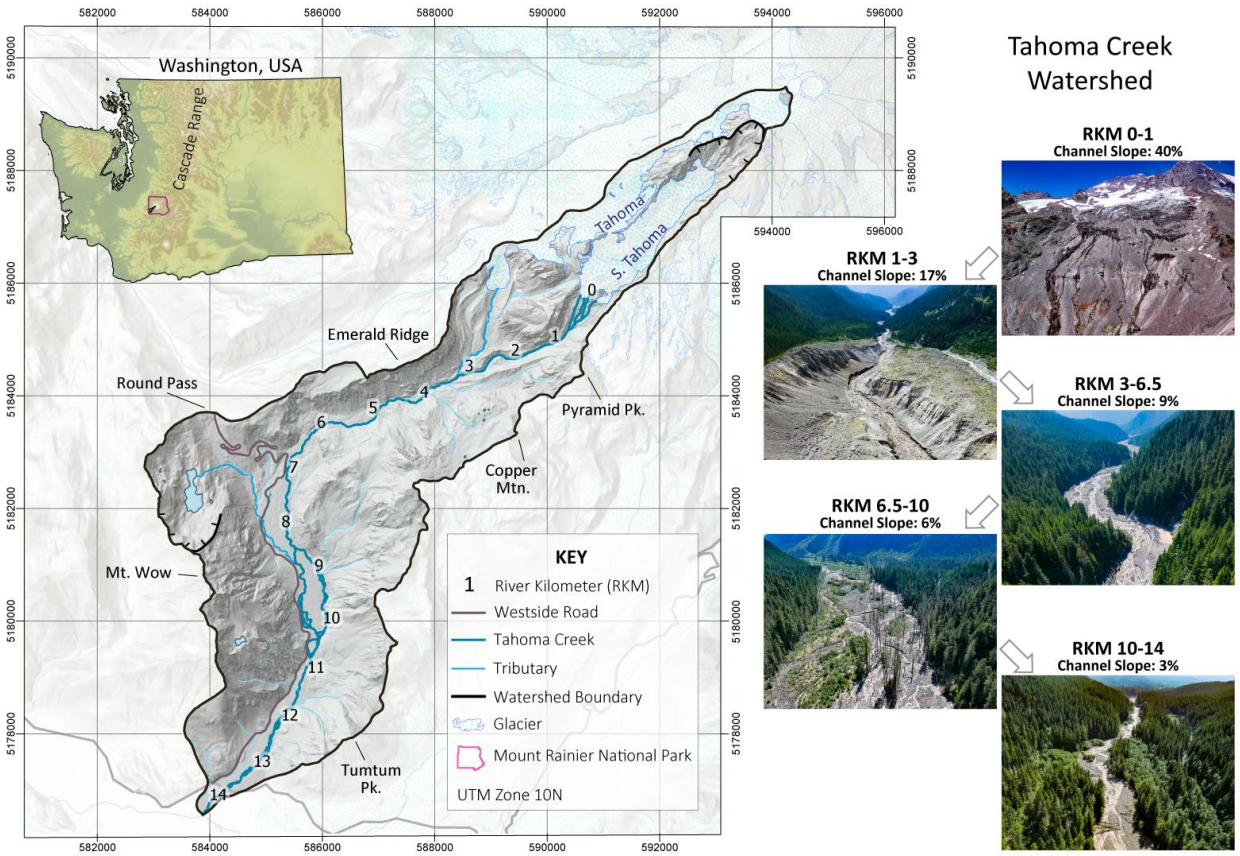

Figure 1: Location map of the Tahoma Creek watershed with selected photos of key valley segments (modified from Turley et al., 2021).

path beginning as multiple meltwater channels flowing over volcanic bedrock ribs and patchy Neoglacial sediments (RKM 0-1, 40% channel slope) before flowing through a deeply incised, narrow canyon of unconsolidated drift (RKM 1-3, 17% channel slope). As the river exits the proglacial zone (zone within the Little Ice Age extent; Carrivick & Heckmann, 2017) it is joined by a tributary issuing from a small lobe of the Tahoma Glacier and flows through a moderately confined canyon flanked by forested hillslopes (RKM 3-6.5, 9% channel slope). This canyon eventually gives way to a broad unconfined valley characterized by mixed terrace, floodplain, and active channel components with dead tree stands recording recent aggradation and channel widening (RKM 6.5-10, 6% channel slope; Walder & Driedger, 1994ab; Anderson & Pitlick, 2014; Turley et al., 2021). The channel narrows once more and is confined by paired terraces (RKM 10-14, 3% channel slope) before spilling out on a debris fan that joins the Nisqually River.

2.1 A History of Dynamic Change

The contemporary dynamic landscape is primarily the result of episodic andesite lava flows building impressive topographic relief (Fiske et al., 1963) and repeated cycles of glaciers carving valleys, oversteepening valley walls, and leaving behind large volumes of unconsolidated material (Crandell & Miller, 1974). Infrequent, although not rare, large sector collapse events that mobilize into cohesive lahars are known to occur (Crandell, 1971; Scott et al., 1995). These large events, which are typically on the order of 10^8 m^3 in volume, are estimated to have a recurrence interval in the range of 500-1000 years for Mount Rainier (mountain-wide), while three events of similar magnitude have occurred within the Tahoma Creek watershed within the last 6,800 years (Scott et al., 1995).

Today, the Tahoma Creek watershed is prone to frequent non-cohesive debris flows, typically on the order of 10^4 to 10^5 m^3 in volume, that enact rapid geomorphic change (Walder & Driedger, 1994a). At least 35 debris flow events have occurred since 1967 (Richardson, 1968; Crandell, 1971; Walder & Driedger, 1994a, 1994b; Legg et al., 2014; Beason et al., 2019). These events often originate as glacial outburst floods, or failure of proglacial gully walls during hydrological events (Walder & Driedger, 1994a; Legg et al., 2014). Beason et al. (2019) describe the debris flow hazard model used at Mount Rainier to forecast both dry and wet weather debris flows with some success.

In November of 2006, a large atmospheric river dropped around 500 mm of rain (maximum rainfall intensity of 20 mm hr^{-1}) on bare slopes over a 3-day period, an amount far higher than any other event since 1920 when records began (Legg et al., 2014; Anderson & Shean, 2021). This event in turn triggered widespread flooding, debris flows and landslides, factoring in heavily to the quantitative sediment budget presented in this study. This dynamic history and spatially heterogeneous nature make the Tahoma Creek watershed an ideal location for this study.

3 Methods

3.1 Mapping

Sediment storage landforms, which are physical representations of sediment disconnectivity in the landscape, were mapped in the field at a 1:8,000 scale during the summer of 2019 following

criteria outlined by Riedel and Dorsch (2016). The upstream affected areas were then estimated based on D8 flow routing using GIS software with the delineated landforms set as targets. Low-gradient areas were defined as having slopes less than or equal to 8 degrees, a slope threshold found to perform well in this watershed (Turley et al., 2021). Both the flow routing and slope estimates were calculated using the 2008 lidar downsampled to 5-meters resolution, which Turley et al. (2021) found to best capture real disconnections. Vegetation was mapped from 1-meter ortho NAIP (National Agriculture Imagery Program; USDA, 2019) imagery collected in 2009 through the calculation of the normalized difference vegetation index (NDVI) using a field-verified threshold. Sources of disconnectivity are classified based on the system proposed by Fryirs et al. (2007a), and encompass buffers, barriers, and blankets which affect the lateral, longitudinal, and vertical disconnectivity, respectively.

3.2 Sediment Budgeting

We present both a conceptual and a quantitative sediment budget over human-timescales (~100 years) for the Tahoma Creek watershed based on a compilation of historical records, published literature (Anderson & Pitlick, 2014; Anderson, 2013), and original contributions from this project. For the conceptual budget, sediment sources, sinks, pathways, and transfer processes were noted in the field during the summer of 2019, and using lidar and NAIP imagery. As an example of this process, sediment sinks/stores (e.g., talus aprons) were mapped. The up-valley sources were also identified (e.g., bedrock outcrops), and the transfer process(es) were inferred based on contextual information and an understanding of process-form relationships (e.g., rockfall). The sources were then categorized as either primary or secondary in nature. The secondary sources category refers to hillslope or valley storage components (sinks) that periodically act as sediment sources, while primary sources are the original stores.

The quantitative budget is based on net change analysis using 1-meter lidar from 2002, 2008, and 2012. We restricted our analysis to the valley floor and adjacent active hillslopes, as determined in the field, to avoid unnecessarily including large areas with insignificant change and increased uncertainties. The resulting budget incorporates fluvial and debris flow processes, and bank erosion. The 2008 and 2012 lidar data cover virtually the entire watershed, while the 2002 lidar covers the active channel and adjacent hillslopes from the glacier front to RKM 12.5. For a more complete description of the datasets see Anderson and Pitlick (2014). The lidar datasets were co-

referenced using a terrain-matching technique (Anderson & Pitlick, 2014). While acknowledging that as a mass balance approach, sediment budgets should include an accounting of water, sediment, solute, and nutrient fluxes, and that anything less may seriously limit its quality (Slaymaker, 2004) this project is restricted to a description of the coarse fraction of sediment due to data limitations. However, we suggest that this is an acceptable limitation because we are primarily concerned with land-forming materials (coarse sediment), which have been the focus of past literature at Mount Rainier.

3.2.1 Sources of Uncertainty

The random error and systematic error (DEM-based) uncertainties were calculated for each of the sediment budget components following methods outlined in Anderson and Pitlick (2014) and using the Westside Road (Figure 1) as a stable reference location. The random error uncertainty (σ_{re}) was estimated by calculating the standard deviation of unresolved errors between the 2002 and 2012 road surfaces. In our case, σ_{re} was roughly 0.08 m, which was conservatively increased to 0.3 m, consistent with values from Anderson and Pitlick (2014). Random error uncertainty was estimated as, $\sigma_{re}\sqrt{A}$, where A is the area of interest in m^2. Because the area of interest was sufficiently large, the random error component of uncertainty was negligible and was excluded from the final estimates.

The systematic uncertainty (σ_{sys}) was estimated by calculating the unresolved mean elevation differences between the 2002 and 2012 road surfaces. In our case, σ_{sys} was approximately 0.017 m, which we increased to 0.025 m to account for the increased uncertainty for measurements within the cobble-boulder channel, consistent with Anderson and Pitlick (2014). The systematic uncertainty of a given area A is, $\sigma_{sys}A$.

In addition to DEM-based uncertainty, several other sources of uncertainty exist. Surface lowering associated with the melting of disconnected stagnant ice is likely the single most important source of uncertainty. Areas where aerial imagery or the patterns of surface lowering suggested the presence of buried stagnant ice were excluded from the analysis. Additionally, some sediment sources may have been excluded from the defined limits of the DEM of difference (DoD) analysis. For example, some coarse sediment enters the system at the glacier front, but this source is assumed to supply much less sediment than other proglacial sources (Fahnestock, 1963). A large proportion of the sediment directly entering the proglacial channels is likely suspended and dissolved load that is readily exported from the basin causing minimal

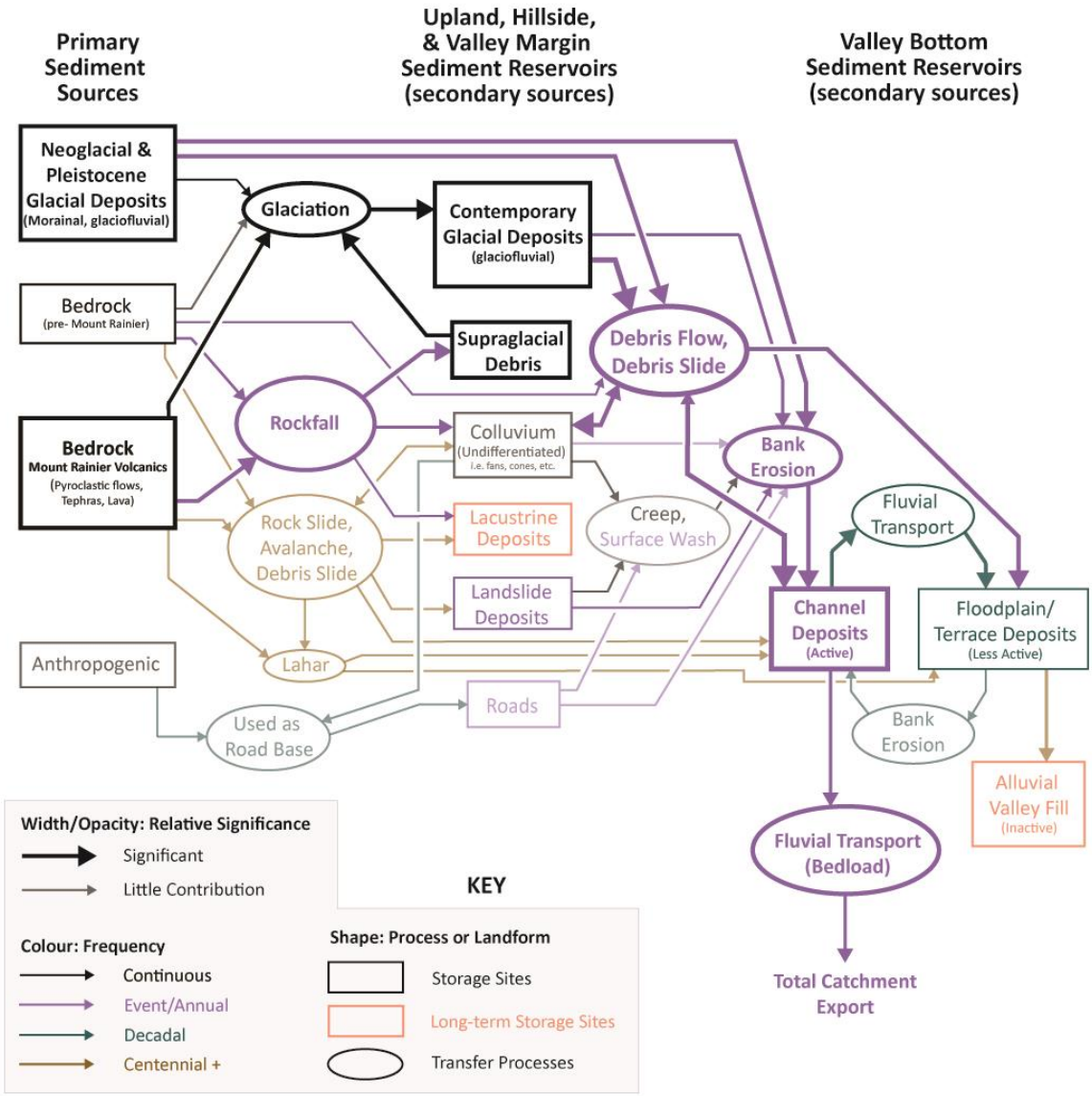

Figure 2: Conceptual coarse sediment budget of the Tahoma Creek watershed.

morphological change. Nevertheless, fine sediment accumulations in backwater areas or floodplains are not uncommon and complicate the assumption that all morphological changes can be attributed to coarse sediment. Minor hillslope sediment sources may have also been excluded from the analysis. However, fieldwork during the summer of 2019 suggested that little sediment entered the channel from the forested hillslopes, a conclusion supported by Anderson and Pitlick (2014). Density differences between eroded sediment and re-stored sediment contributes to additional uncertainty, although is likely less important than those previously mentioned.

4 Results

4.1 Qualitative and Conceptual Sediment Budget

In constructing a sediment budget for the Tahoma Creek watershed, we attempt to assess the relative importance of various processes of sediment transfer and the causes of disconnectivity within the watershed. Significant sources, sinks, and pathways will be discussed in the following paragraphs, while a more complete accounting is conceptualized in Figure 2.

4.1.1 Sources

4.1.1.1 Primary Sources

The primary sources of sediment within the Tahoma Creek watershed include bedrock (both pre-Mt. Rainier and Mt. Rainier volcanics), glaciogenic sediment, and sediment synthetically added to the system, primarily for road repair (Figure 2). While volcanic eruptions add new volumes of rock and ash, the last know eruption of Mount Rainier occurred 550 to 600 years ago, well outside of the timescale of this study (Fiske et al., 1963). Andesite of the Mount Rainier volcanics outcrops above the glacier termini in the headwall of the South Tahoma Glacier, along the bedrock ridges dividing the Tahoma, South Tahoma, and Pyramid glaciers, and along many of the ridges forming the watershed divide. This bedrock is the main source of glacial debris. Pre-Mount Rainier bedrock, including the Ohanapecosh and Stevens Ridge Formations as well as intrusive granodiorites and quartz monzonites, dominate the watershed below the glacier termini. Unsurprisingly, basal and ablation till as well as glaciofluvial sediment makes up most of the sediment in the proglacial zone. These primary glacial deposits are easily delineated by the prominent LIA lateral and end moraines. Glaciogenic sediment is the most significant and active source within the watershed at the human-timescale.

4.1.1.2 Secondary Sources

Secondary sources of sediment within the watershed are abundant owing to paraglacial (and proglacial) sedimentation occurring within the valley train and on the adjacent hillslopes. The secondary sources can be further divided into two broad categories in terms of the primary source they are generally derived from and their valley position. The first grouping of secondary sources, those that are primarily derived from bedrock, includes debris avalanche deposits, rock fall deposits, talus, debris cones, and undifferentiated colluvium. These sources generally lie along the lower flanks of the hillslopes and at the hillslope-valley bottom transition. Eight mass movement deposits were mapped within the watershed, five of which are periodically eroded as the river shifts course and undercuts the landforms causing slumping. Undifferentiated colluvium consisting of weathered rock, debris, soil, and vegetation is sourced in the same way. Debris cones lie at the hillslope-valley bottom transition and are sourced through lateral incision at the toe or longitudinal incision by the tributary stream. Talus generally lies higher on the hillslopes directly below rocky cliffs, and seldomly reaches the valley floor. Talus becomes a source of sediment in locations where bedrock outcrops proximal to the valley floor.

The second grouping of secondary sources, derived primarily from glaciogenic sediment within the proglacial zone, includes the active channel, floodplain, terrace, alluvial fan, and debris fan deposits. Debris flow levees would also fit into this category but are relatively less voluminous. Situated on the valley floor, sediment is exchanged between these secondary sources on a regular basis as the river shifts course.

4.1.2 Sinks / Sediment Storage

The secondary sources previously listed alternatively act as sediment sinks. Sediment sinks either partially or completely prevent the transfer of sediment through the system. Different storage landforms operate over varying effective timescales (Fryirs et al. 2007a; Harvey, 2002). For example, within the watershed, lakes are highly effective sediment sinks and operate over millennial timescales. Valley floor aggradation also leads to inactive valley fill deposits that may remain in storage for centuries to millennia. Other sediment storage reservoirs include colluvium (i.e., undifferentiated-debris cones and fans, talus), landslide deposits, alluvial fans, terraces, floodplains, and the active channel.

310 4.1.3 Pathways – Sediment Production and Transport Processes

311 Sediment production and transport processes route sediment from source to sink. Figure 2
312 summarizes the sediment pathways noting the relative significance, and frequency of each
313 process. Frost wedging/shattering occurs throughout much of the year and leads to high rates of
314 rockfall, especially within the South Tahoma Glacier headwall. Approximately 0.56 km^2 of the
315 South Tahoma Glacier's surface was covered in debris in 2015 (Beason, 2017). Glaciers mediate
316 the transfer of rockfall from cirque headwalls to the terminus through slow, continuous transport
317 providing a buffering effect and long-term storage of debris. Erosion primarily occurs within the
318 proglacial zone. During periods of moderate and low magnitude floods, sediment is mainly
319 sourced from the proximal slopes of lateral moraines through periodic gullying at or near the
320 moraine crest and is then temporarily stored along the base in cones or sheets. Shallow
321 translational slides originating near the moraine crest are also likely common (Curry et al.,
322 2009). During larger magnitude floods and debris flows, the sediment accumulations at the base
323 of the moraines are eroded and contribute to bulking of debris flows. Over human-timescales,
324 debris flows, and fluvial bank erosion are the two most important processes coupling hillslope
325 sediment sources to the valley floor and eventually the catchment outlet.

326 Many of the other processes only become significant over much longer timescales including
327 debris avalanches/slides, lahars, and soil creep/tree throw. For example, soil creep and tree throw
328 act over a large area, but at slow rates. These factors make it difficult to directly measure rates in
329 the field, and as such, none were attempted. Jordan and Slaymaker (1991) note a combined
330 average soil creep/tree throw rate of 2-5 mm y^{-1} for shallow (0.5 - 1m), forested soils in
331 mountainous settings. The drainage density of the Tahoma Creek watershed is approximately 2.8
332 km per km^2, while field estimates suggest that less than 5.5 km^2 of soil-mantled slopes are
333 coupled to the valley floor. Based on the above values, soil creep volumetric estimates range
334 between 15 m^3 y^{-1} to 80 m^3 y^{-1} (1.5 to 8 x 10^3 m^3 in the last 100 years). As will be shown in the
335 following paragraphs, soil creep estimates are within the uncertainty bounds of more significant
336 processes (i.e., fluvial erosion, debris flows) within the watershed.

337 4.2 Quantitative Sediment Budget from Multitemporal Lidar

338 Figure 3 illustrates the estimated coarse sediment budget between 2002-2008 and 2008-2012
339 based on the DoD analysis, while Table 1 presents averaged annual volumes for comparison

(Turley & Hassan, 2023). Between 2002 and 2008 at least 3232 ± 35.4 x 10^3 m^3 of sediment was eroded and 1734 ± 33 x 10^3 m^3 of sediment was deposited within the valley floor. Roughly 80% of the total erosion occurred within the proglacial zone (RKM 0-3), while ~85% of the total deposition occurred between RKM 3-10.5. During this period, an estimated 1498 x 10^3 m^3 (250 x 10^3 m^3 y^{-1}) of coarse sediment was exported from the watershed.

In contrast, between 2008 and 2012 a minimum of 840 ± 22.4 x 10^3 m^3 of sediment was eroded and 696 ± 27.2 x 10^3 m^3 was deposited within the valley floor. Approximately 70% of the total erosion occurred within the proglacial zone, while 50% of the deposition occurred between RKM 3-10.5. During this period, only 144 x 10^3 m^3 (36 x 10^3 m^3 y^{-1}) of sediment was exported from the watershed.

Table 1: Averaged annual volumes of erosion, deposition, and total export for the Tahoma Creek Watershed based on the analysis of DEM's of difference for the two periods (2002-2008, and 2008-2012). The sediment delivery ratios (SDR) are also presented for the two periods.

Period	2002-2008	2008-2012
	Avg. Annual Volume (x 10^3 m^3)	
Gross Erosion	539 ± 5.9	210 ± 5.6
Gross Deposition	289 ± 5.5	174 ± 6.8
Total Export (net change)	250 ± 11.4	36 ± 12.4
SDR	46%	17%

4.2.1 Sediment Delivery Ratios

The sediment delivery ratio (SDR) was calculated every 3-4 kilometers for both periods based on the net export of sediment past a point divided by the gross erosion upstream of that point (Figure 3; Turley & Hassan, 2023). The gross erosion volumes are minimum estimates only and therefore the delivery ratios are maximum estimates. The SDR from the proglacial zone (RKMs 0-3) is 94% for the period 2002-2008, and 61% between 2008 and 2012. The lower delivery ratio in the latter period is a reflection of sediment re-stored at the base of the lateral moraines. The SDR drops to 71% and 43% between RKMs 3-6.5 for the periods 2002-2008 and 2008-2012, respectively. The SDR further drops to 48% and 22% between RKMs 6.5-10 for the 2002-2008

and 2008-2012 periods, respectively. This amounts to approximately a 40% decrease in the SDR between RKMs 3-10.5 for both periods, reflecting the largely depositional nature of this area. Downstream of RKM 10.5 the SDR changes relatively little with erosion approximately balancing out deposition. For the period 2002-2008 the SDR dropped a mere 2% (down to 46%) by RKM 12.5 where the DoD coverage ends. For the 2008-2012 period the SDR is reduced by 1% and then an additional 4% (down to 17%) between RKMs 10.5-12.5 and 12.5-14, respectively. The resulting 25% difference in SDR, as measured at RKM 12.5, between the two periods is largely a result of the temporary storage of eroded sediment at the base of the lateral

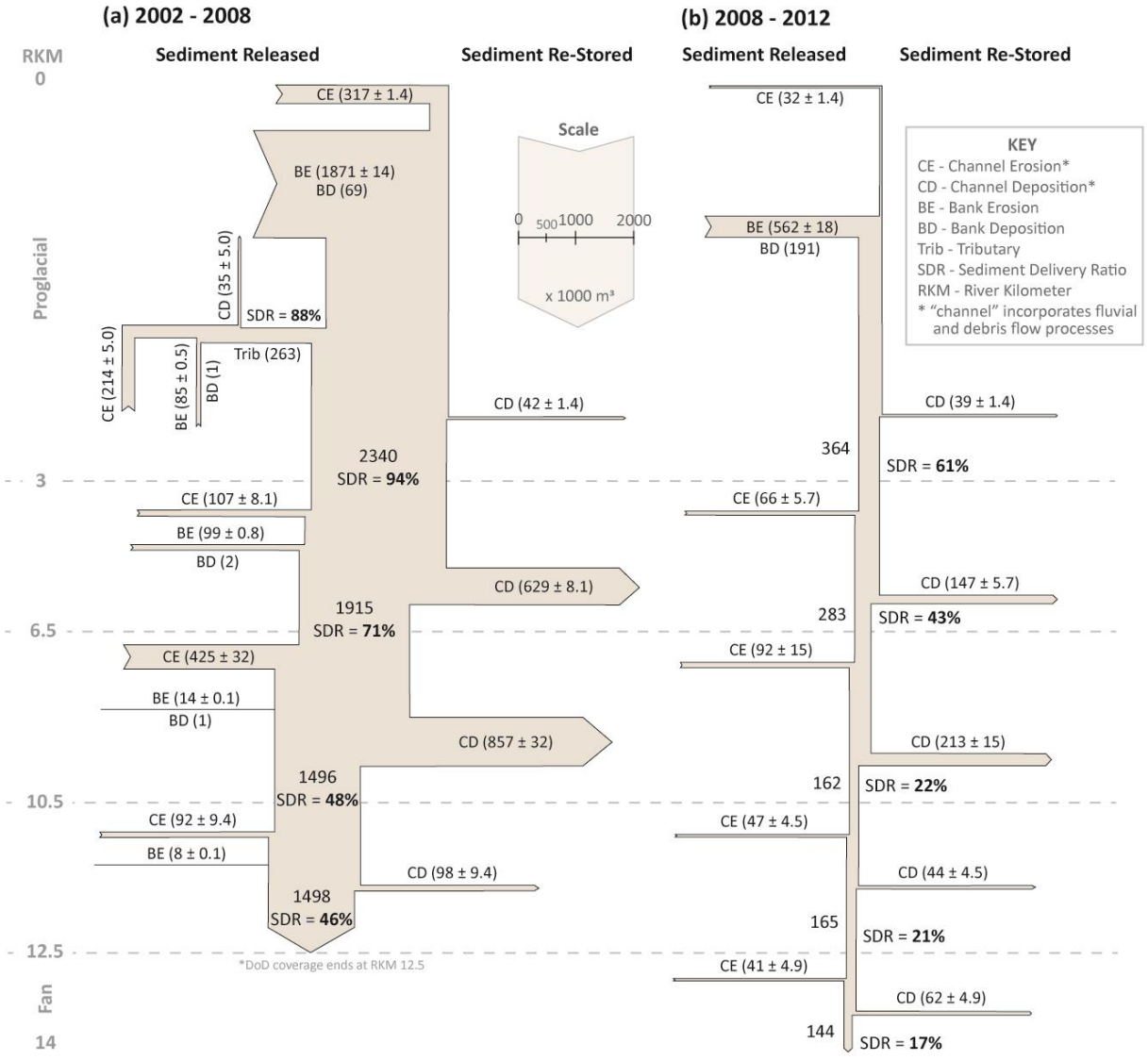

Figure 3: Sediment budget for the Tahoma Creek watershed during the (a) 2002 to 2008 period, and the (b) 2008 to 2012 period. Sediment volumes measured from consecutive 1-meter lidar datasets cropped to the active channel and contributing hillslopes. Incorporates fluvial, debris flow, and bank erosion processes.

372 moraine within the proglacial zone. All other erosion/deposition patterns within each zone
373 remained similar between the two periods.

374 4.3 Sources of Disconnectivity

375 Disconnectivity is the dominant but inefficient state of a system in transferring matter and energy
376 within and between system components. Sources of sediment disconnectivity are therefore
377 landforms or bio-geomorphic characteristics of the system (i.e., vegetation, slope, network
378 structure, etc.), that reduce the efficiency of sediment transfer through storage. Table 2 provides
379 a general overview of the landforms and bio-geomorphic characteristics that were identified and
380 includes a description of their effects on disconnectivity.

381 The features identified include lateral moraines, debris flow levees, low gradient areas, lakes,
382 vegetation, terraces/floodplains, fans/cones, roads/culverts/bridges, grain size and competence,
383 in-stream large wood, valley constrictions, and sediment slugs. The location and upstream
384 affected areas of each of the sources of disconnectivity identified within the Tahoma Cr.
385 watershed are visualized in Figure 4 and the respective statistics are summarized in Table 3.
386 Much of the hillslopes and valley bottom terraces are densely forested, while geomorphically
387 active areas often lack vegetation. This results in an estimated 57% of the watershed being
388 vegetated including bedrock areas (Table 3). Low gradient areas are primarily located on the
389 valley bottom, but also include hillslope features such as breached divides, cirque floors, and
390 parklands (i.e., low gradient surfaces composed of ancient lava flows scoured by glacial erosion;
391 Riedel & Dorsch, 2016).

392 Lateral moraines delineate the proglacial zone from RKM 0-3.5 and disconnect ~2% of the
393 watershed. Terraces and floodplains are the two landforms that disconnect the largest proportion
394 of the watershed at 34% and 23% of the total area, respectively (Table 3). They are
395 discontinuous in the upper watershed and become prominent where the valley widens (RKM
396 6.5), remaining nearly continuous to the outlet. Debris cones and fans, which range in size from a
397 few tens of square meters to nearly a square kilometer, are primarily located between RKMs 7.5
398 and 12 and together affect approximately 9% of the total basin area (Figure 4; Table 3). Lakes
399 disconnect around 7% of the watershed, with the two biggest being tarns located in glacial
400 cirques in the eastern portion of the basin (Figure 4; Table 3).

401 **Table 2: Description of how specific landforms and bio-geomorphic characteristics increase disconnectivity in (post)glacial**
402 **watersheds. Includes selected photographs from the Tahoma Creek watershed as examples – taken during the 2019 field**
403 **season. Photos of fans, valley constrictions, and sediment bulges courtesy of Taylor Kenyon, NPS.**

Landform / Characteristic	Description	Effect on Disconnectivity	Photo
Lateral moraines	Sharp crested linear accumulation of glacially transported rock and debris dropped by the ice along its' lateral margins as it melts.	Cause localized deposition of hillslope sediment on the distal slope of the moraines, while the proximal slope often acts as a sediment supply.	
Debris flow levees	Shear related boundary features resulting from non-cohesive debris flows (Scott et al., 1995). Linear accumulations of sediment that may contain large, downed trees and boulders more than 2 meters across.	Temporarily inhibit the lateral migration of the river, and if located near the valley margin, may prevent hillslope sediment from entering the channel.	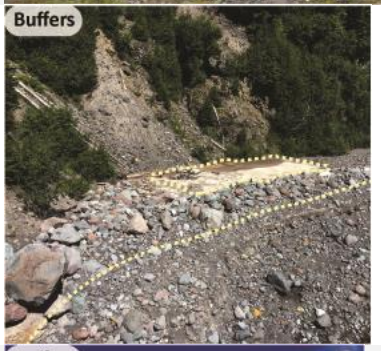
Low gradient	Definitions will vary widely. Defined here as surfaces with < 8° gradient. Hillslope features may include parklands, cirque floors, breached divides, etc. Valley bottom features may include terraces, floodplains, etc. (see other sections).	Results in reduced potential gravitational energy available for sediment transport processes that favor deposition over transport when slope thresholds are not surpassed.	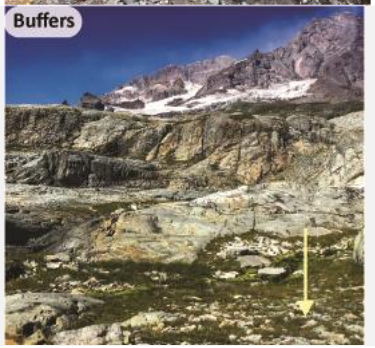

Landform / Characteristic	Description	Effect on Disconnectivity	Photo
Lakes	Relatively large body of slowly moving or standing water surrounded by land.	Effectively disconnect all upstream areas with respect to coarse sediment, and likely trap a high proportion of the suspended sediment.	
Vegetation	Plants and plant life of an area taken as a whole.	Reduces erosion and promotes deposition and storage by increasing the surface roughness and infiltration, and stabilizing and trapping sediment (Cienciala, 2021).	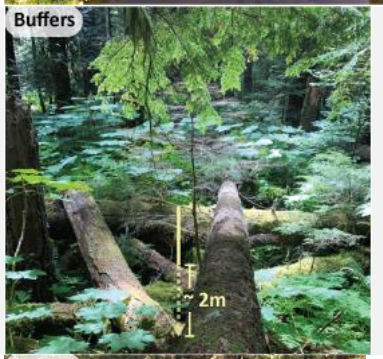
Terraces / floodplains	An area of low-lying ground adjacent to a river, formed mainly of river sediments and subject to flooding (Floodplain). Former floodplain surface now elevated above the contemporary channel (Terrace).	Cause localized deposition at the hillslope-valley bottom transition. These landforms are low gradient, and often vegetated (see other sections).	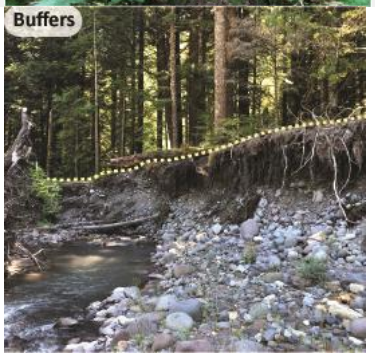

Landform / Characteristic	Description	Effect on Disconnectivity	Photo
Fans / cones	Fan- or cone-shaped landforms at the hillslope-valley bottom transition composed of sediment deposited by fluvial or mass movement processes.	Buffer hillslope sediment through deposition as the slope decreases. Leenman and Tunnicliffe (2020) identified the key up- and downstream controls on fan evolution and buffering capacity as, sediment supply and stream power (upstream), and mainstem aggradation and distal confinement (downstream).	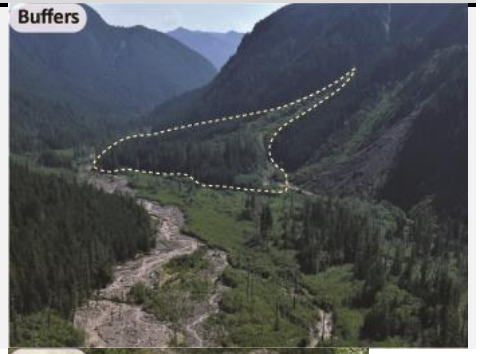
Roads / culverts / bridges	Anthropogenic infrastructure including flat surfaces prepared for transportation (roads), over a river or other obstacle (bridge), or artificial surface water drainage routing (culverts).	Road's cause localized deposition on the upslope side of roadway due to break in slope. Culverts and bridges limit the lateral mobility of streams and may create backwater areas resulting in deposition upstream of the constriction.	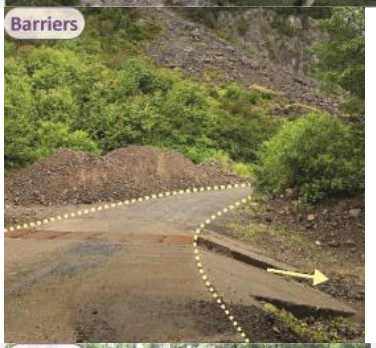
Grain size / competence	Mass movement and glacial processes are not size selective – sediment delivered to the channel may be too large to be transported.	Sediment transfer processes vary in their capacity to transfer coarse sediment (e.g., boulders). Persistent aggradation of coarse sediment may occur at the transition between process domains when processes that are not size-selective (e.g., debris flow) supply sediment to processes that are (e.g., fluvial). The degree of longitudinal disconnectivity is controlled by the relation between grain size and river competence. Note that this can also result in blankets (discussed below).	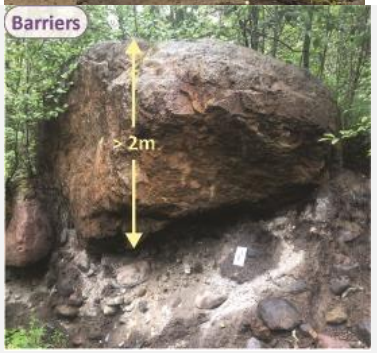

Landform / Characteristic	Description	Effect on Disconnectivity	Photo
In-stream Large Wood	Logs, sticks, and branches and other wood that protrude or lay within the channel. Generally, > 10 cm in diameter.	Channel spanning log jams create areas of backwater and sediment wedge accumulation. Dead standing trees increase flow resistance and may trap wood and sediment. Large wood often accumulates at the bouldery, and debris-filled snout of debris flows and aids their deposition through increased flow resistance.	
Valley constrictions	Relatively narrow section of the valley bottom. May be the result of glaciation, incision, debris fan progradation, deep-seated landslides entering the valley bottom, etc.	Prevent the river from migrating laterally and can cause backwater areas and aggradation upstream as a result of the bottleneck effect. Alternatively, may act as a 'booster' that concentrates flow through a narrow area and enhances sediment conveyance through this reach.	
Sediment bulges / slugs	Large fluxes of sediment that can act as plugs within the active channel during low to moderate flows, and thereby limit downstream sediment transport (Nicholas et al., 1995; Fryirs et al., 2007a). May be the result of a single event (e.g., landsliding) or long-term incremental input at a range of spatial scales.	Limit the vertical reworking of sediment by effectively smothering other landforms. Sediment pulse evolution is in part controlled by network structure (Benda et al., 2004), which can enhance or disperse the pulse as a result of synchronization and translation or desynchronization and storage, respectively (Gran & Czuba, 2017).	

404

405
406 **Table 3: Summary statistics of landforms and bio-geomorphic characteristics**
407 **identified within the Tahoma Cr. watershed and their upstream affected areas.**

Landform/ Characteristic	Coverage Area (km^2)	Upslope Affected Area (km^2)	Percent Total Area Affected[a]
Terraces	1.39	9.7	34%
Floodplains	0.86	6.82	23%
Lakes	0.17	1.97	7%
Debris Cones	0.36	1.45	6%
Alluvial Fans	0.04	0.8	3%
Parkland[c]	1.05	-	3%
Moraine Crests	-	0.7	2%
Vegetated[b,c]	~18.7	-	57%
Slope < 8°[c]	3.64	-	11%
Slope < 4°[c]	1.43	-	4%
Slope < 2°[c]	0.5	-	2%
Total Area Below Glacier Limits (km^2)	32.9		

[a]Based on the actual coverage and upslope affected area of each source of disconnectivity in relation to the total catchment area (below glacier limits). Note that a given location may be affected by more than one landform/characteristic (sum total exceeds 100%).
[b]Based on manually verified normalized difference vegetation index (NDVI) value.
[c]Upslope affected area not calculated for parkland or catchment characteristics. Percent total area affected is based on coverage area only.

408

409 **5 Discussion**

410 The link between contemporary processes operating on a mountainous glacial landscape, the
411 presence of sources of disconnectivity, and the resulting spatial patterns of sediment dynamics
412 and transfer efficiencies is poorly understood. In this paper, we calculate a sediment budget for
413 two time periods using high-resolution multi-temporal lidar data and identify and map sources of
414 disconnectivity for a 40 km^2 watershed to explore this link. These unique datasets illustrate
415 catchment-scale sediment dynamics and transfer efficiencies, the role of extreme events, and the
416 effective timescales of sources of disconnectivity, each of which are discussed in more detail in
417 this section.

418 5.1 Downstream Trends of Lateral and Longitudinal Disconnectivity

419 The Tahoma Creek watershed is incredibly dynamic as a result of impressive topographic relief,
420 large stores of unconsolidated glacial sediment in the headwaters, and retreating glaciers that

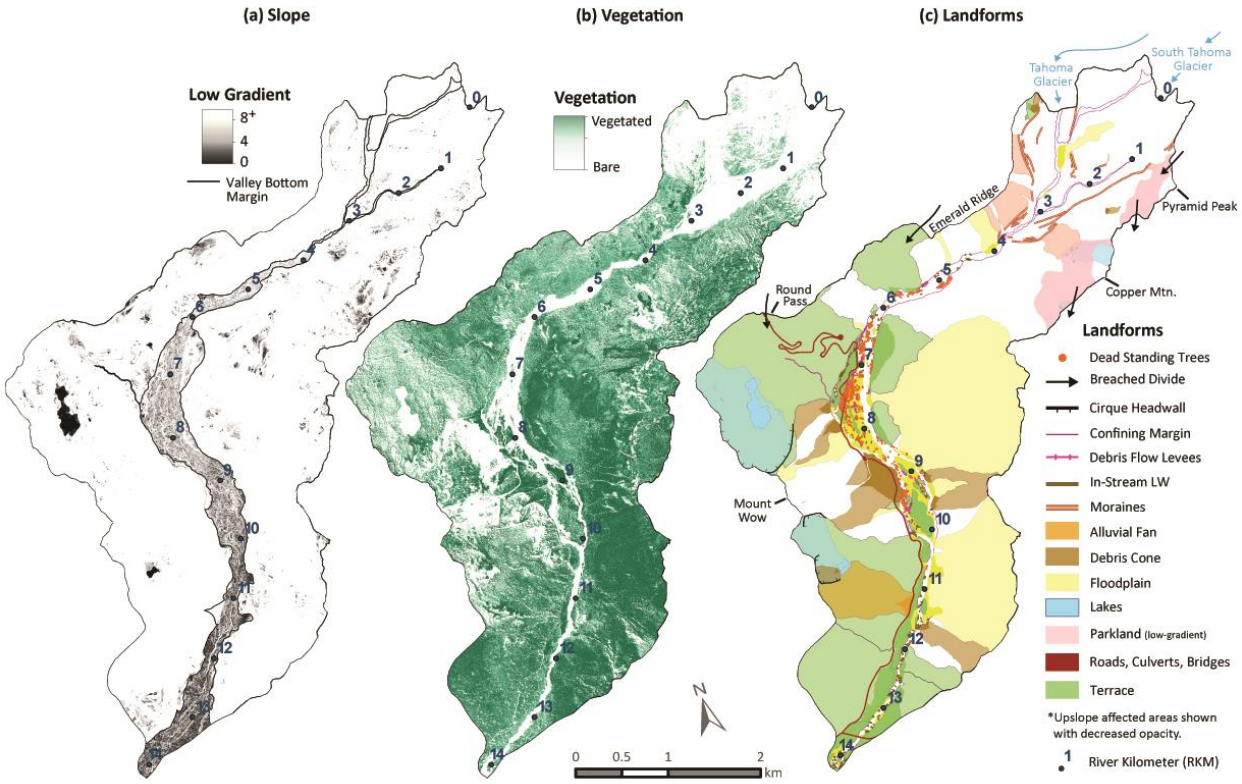

Figure 4: Map of sources of disconnectivity and their upstream affected areas within the Tahoma Creek watershed. Sources of disconnectivity visualized include (a) slope and (b) vegetation – both characteristics of the system, and (c) landforms with their upslope affected areas. The upstream affected areas are based on D8 flow routing and are displayed in the same color as their associated landform with transparency added. Areas that remain in white are high gradient, unvegetated, or are not directly affected by the landforms that increase disconnectivity.

produce glacial outburst floods and debris flows. However, the spatial patterns of sediment sources, pathways, and sinks suggest that the majority of the watershed is in a state of disconnectivity over human timescales. Active sediment sources that are coupled to the channel are primarily limited to the proglacial zone (RKM 0-3), which supplies up to 80% of the total sediment. Sources of disconnectivity affect less than 10% of the proglacial area (Figure 5a) which results in the efficient transfer of eroded sediment, especially during large events (SDR ~94%). This is in direct agreement with several semi-quantitative indices of connectivity (Figure 5b; Turley et al., 2021). The indices applied by Turley et al. (2021), and used as reference in this text, include hillslope-channel coupling (Whiting & Bradley, 1993), the effective catchment area (ECA; Fryirs et al., 2007b), the index of connectivity (IC; Cavalli et al., 2013), the joint index of connectivity (IC_j; Ortiz-Rodriguez et al., 2017), network structural connectivity (NSC; Cossart & Fressard, 2017), residual flow (RF; Fressard & Cossart, 2019), and the spatially distributed sediment delivery ratio (SD SDR; Heckmann & Vericat, 2018).

Down valley, disconnectivity becomes increasingly more prevalent. Between RKMs 3-5 the cumulative percent area affected by sources of disconnectivity reaches a moderate 40-60%, the channel becomes net depositional, while the hillslopes remain predominantly coupled to the channel (Figure 5). Between RKMs 5-7 in-channel deposition increases reducing the SDR by another 20%, the hillslopes become decoupled from the active channel (~RKM 6; Figure 5b), and the cumulative percent area affected by sources of disconnectivity reaches 100%. Interestingly, all of the low gradient landforms within the hillslope are a direct result of glaciation (i.e., parklands, breached divides, cirque floors) and significantly increase the cumulative disconnectivity. This supports work by Hoffmann et al. (2013) which suggests glacial cirques disconnect glacial headwater basins from main river valleys.

Below RKM 7 disconnectivity reaches a maximum with the cumulative percent area affected by sources of disconnectivity reaching 190%, suggesting that most locations are affected by 2 or more sources of disconnectivity (i.e., terraces, vegetation, low gradient). Between RKMs 7-10 a substantial amount of in-channel deposition occurs causing the channel to aggrade and reducing the SDR to 22-48%. Over the last half century, this has resulted in several meters of uniform valley aggradation (Walder & Driedger, 1994a; Anderson & Shean, 2021). Below RKM 10, continuous paired terraces completely decouple the hillslopes from the active channel, and connectivity estimates reach a minimum (Figure 5).

The spatial distribution of sources of disconnectivity explains, to a large degree, the structural sediment connectivity estimated by Turley et al. (2021), and functional connectivity or catchment-scale sediment dynamics from this study (e.g., SDR). The main exception to this finding is the contrasting degrees of functional connectivity between the South Tahoma Glacier meltwater channel (mainstem, RKMs 0-3) and the Tahoma Glacier meltwater channel (primary tributary). In this case, debris flows and outburst floods in the mainstem result in significant geomorphic change and functional connectivity, neither of which occur in the tributary valley (Anderson & Shean, 2021). Perhaps unsurprisingly, structural connectivity indices (Turley et al.,

460 2021) were also unable to differentiate between the contrasting degrees of functional
461 connectivity of these two areas. Vegetation, terraces, and floodplains affect the largest portion of
462 the watershed, while lakes are more permanent sediment sinks.

463 5.2 The Role of Exceptional Events

464 Several researchers have stated that in proglacial settings the sequencing of extreme events,
465 rather than more frequent lower-magnitude events (e.g., annual rainfall), controls erosion and

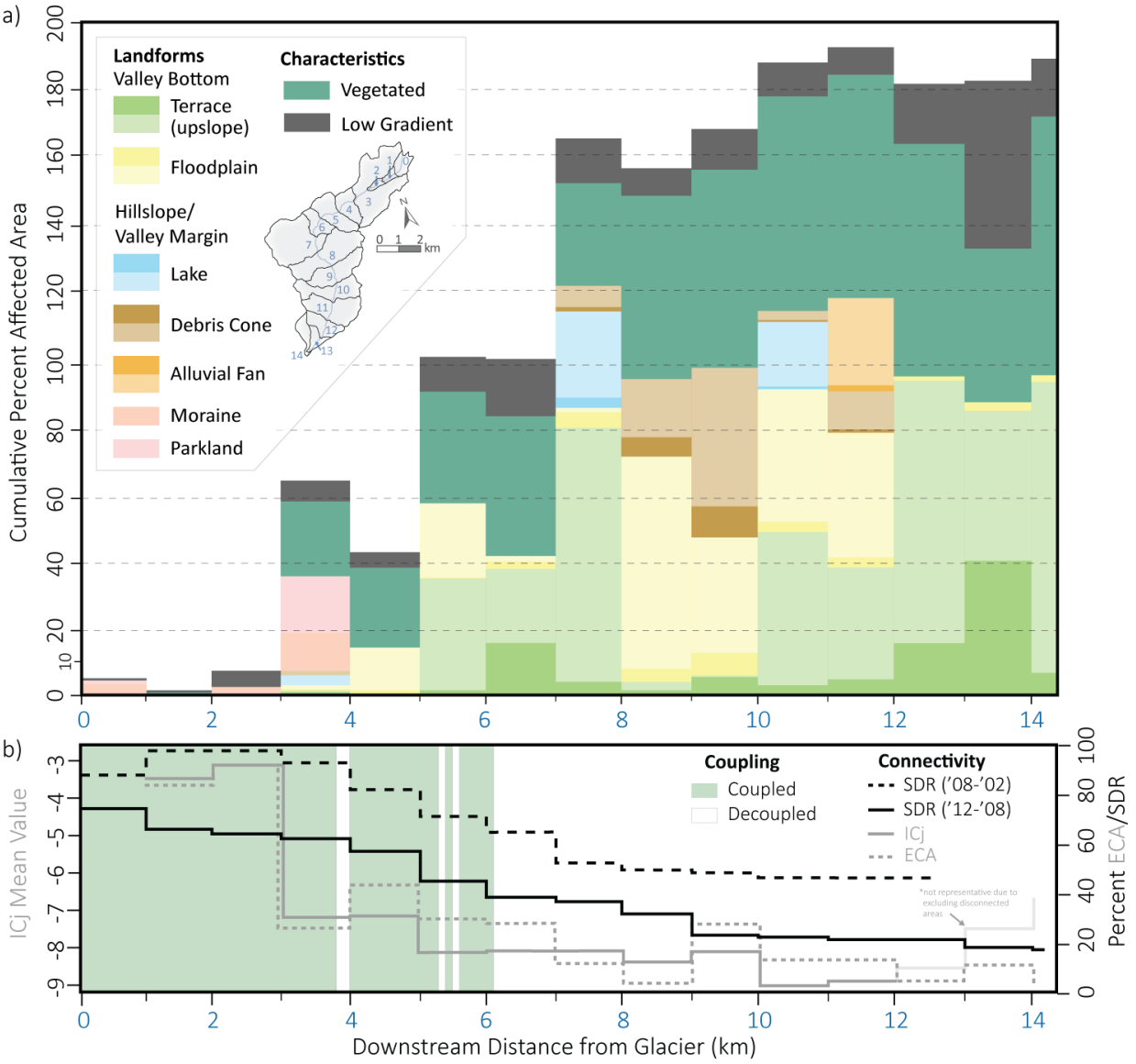

Figure 5: (a) cumulative percent affected area by sources of disconnectivity, and (b) longitudinal pattern of connectivity and hillslope channel coupling (modified from Turley et al., 2021). The colors in (a) correspond to figure 4 (this text). Upstream affected areas are displayed in the same color as their associated landform with transparency added. In panel (b) ICj refers to the joint index of connectivity method (Ortiz-Rodriguez et al., 2017), and ECA refers to the effective catchment area method (Fryirs et al., 2007b).

sediment export over periods of decades and longer (e.g., Anderson & Shean, 2021; Micheletti & Lane, 2016). This conclusion is well supported by evidence from the Tahoma Cr. watershed. The proglacial zone along the mainstem has undergone persistent erosion since 1960, resulting in 50-80 meters of incision along the ~2 km section of channel (Anderson & Shean, 2021). Walder and Driedger (1994a) document two periods of accelerated erosion. Between 1967 and 1971 at least 8 debris flows scoured the channel by about 5-7 meters. Later, between 1986 and 1992, an additional 15 debris flows/floods occurred and scoured the channel by up to 40 meters. Most of this incision occurred in unconsolidated glacial material. However, Walder and Driedger (1994a) suggest that two debris flows in 1992 scoured a notch into the underlying volcaniclastic bedrock 30-40 meters long and 15-20 meters deep and wide. Debris flows and floods have resulted in the rapid adjustment of the mainstem channel profile to nonglacial conditions.

During the 2002 to 2008 period, an estimated 1.5×10^6 m^3 (250×10^3 m^3 y^{-1}) of sediment was exported from the watershed, while only 1.4×10^5 m^3 (36×10^3 m^3 y^{-1}) of sediment was exported between 2008 and 2012. A large debris flow in 2005, and the large 2006 flood and debris flow event are likely responsible for the near order of magnitude difference in sediment transfer volumes. If we assume that an average of 36×10^3 m^3 of sediment was exported each year during the 2002-2008 period (average for the 2008-2012 period) and that extreme events accomplished the remainder of the sediment export, then as much as 85% of the total sediment exported occurred during these extreme events. This is supported by continuous bed material transport estimates for 1956-2011. Anderson and Pitlick (2014) constructed a synthetic daily hydrograph and two-parameter sediment rating curve for the basin using DoD measurements as volumetric bed material transport values. They estimate that up to 80% of the total bedload transport for the 2002-2012 period, and 50-60% of the total bedload transport for the 1956-2011 period, was accomplished during the 3-day flood in 2006.

Turley et al. (2021) calculated the sediment budget and functional connectivity along the base of the lateral moraines near RKM 2 for both periods (2002-2008, 2008-2012). The volume of exported sediment and functional connectivity estimates were significantly higher for the 2002-2008 period, which they attributed to the high-magnitude flood event in 2006, suggesting event magnitude controls functional connectivity. Our quantitative sediment budget and sediment delivery ratio estimates along the valley bottom support this finding. The delivery ratio at RKM

12.5 (end of DoD coverage) was approximately 25% higher and roughly 10 times as much sediment was transported between 2002 and 2008 compared to the 2008-2012 period.

During the 2006 event, high-intensity rainfall (up to 20 mm hr^{-1}, total of ~500 mm) led to the initiation of debris flows and high river discharges which mobilized large volumes of sediment, overcame sources of disconnectivity (e.g., floodplain, grain size/competence), and relatively efficiently exported the sediment from the watershed. During extreme events, thresholds and sources of disconnectivity are surpassed and the efficiency of sediment transfer increases resulting in rapid adjustment.

While barriers and blankets drastically reduce sediment transfer within the channel (longitudinal and vertical disconnectivity), buffers seem to be even more prominent and affective at modulating sediment export and delaying/disrupting signal propagation from the hillslopes (lateral disconnectivity; Figure 4). In essence, evidence suggests that most of the watershed is in a state of disconnectivity (spatially) most of the time (temporally).

The effect that global warming and glacial retreat will have on sediment dynamics and the importance of sources of disconnectivity isn't entirely clear. However, in documenting debris flow initiation in proglacial gullies during the 2006 flood event at Mt. Rainier, Legg et al. (2014) found slope (channel and hillslope gradient) to be the primary control and suggest that proglacial slopes are often transport limited. Because the glaciers have already retreated onto steep slopes within the Tahoma Creek watershed, debris flow initiation occurs regularly, and large volumes of unconsolidated material, along with easily erodible bedrock provide ample material for downstream bulking. As long as these favorable conditions persist, the frequency of debris flows will likely remain high. In the nearby Nooksack Basin in Washington, Anderson and Konrad (2019) found that regional climate variations resulted in changes in upstream coarse sediment supply and were able to track the signal propagation downstream. Interestingly, in a review article based on the Western US, East and Sankey (2020) found that there is evidence for climate-driven changes to slope stability, but found sediment yields and fluvial morphology were more often linked to nonclimatic drivers. As extreme precipitation events become more frequent, and more precipitation falls as rain due to climate change, the frequency of debris flows, and other sediment transport events may increase.

5.3 Effective Timescales of Disconnectivity

The effective timescales of disconnectivity features in the Tahoma Creek watershed range between the individual event and tens of thousands of years. Many of the same features noted by Fryirs et al. (2007a) are present in the study area, but additional glacial and debris flow-related features are noted. The effective timescale of glacial sources of disconnectivity also ranges widely. For example, the watershed divides were likely last breached in the late Pleistocene during the Salmon Springs Glaciation (Crandell & Miller, 1974) and have undergone little modification since. In contrast, the lateral moraines were formed much more recently during Neoglacial advances in the 16th and 19th centuries (Sigafoos & Hendricks, 1972) and are beginning to be eroded where adjacent to the contemporary channel and will likely operate as buffers on the order of centuries.

Terraces and fans operate as buffers over intermediate timescales. Tree core data from within the watershed suggests that many of the terraces have been stable for several centuries (Anderson, 2013). While recent valley wide deposition (Walder & Driedger, 1994ab) has reactivated many terrace features between RKMs 6 and 10 marked by dead standing trees (Figure 4). Unless valley wide aggradation persists, these terraces will act as buffers for millennia. Researchers have identified both upstream and downstream controls on fan evolution and buffering effectiveness (Leenman & Tunnicliffe, 2020). Key upstream controls are sediment supply and stream power, and key downstream controls are mainstem aggradation and distal confinement. The fans and cones in the Tahoma Creek watershed are fed by ephemeral streams, and therefore downstream (mainstem) controls are likely more important. Valley-wide aggradation and subsequent increased lateral mobility of the mainstem may decrease the buffering effectiveness of these features through erosion of the distal fan margins. Nevertheless, they will remain long-term buffers within the sediment cascade.

In general, within the watershed, blankets operate over shorter timescales than barriers, which in turn operate over shorter timescales than buffers. This is likely the result of buffers often relating to basin-scale macroforms and landforms, both glacial and tectonic in origin, while barriers and blankets are often related more to thresholds, process competence, and smaller more transient biological or anthropogenic structures. As previously noted, the main channel rapidly adjusts both laterally and vertically in response to changing conditions. However, hillslope-channel

555 decoupling and abundant sources of disconnectivity at the valley margins and on the hillslopes
556 delay signal propagation and system response. As a result, hillslope features such as glacial
557 cirques, parkland, and glacial drift deposits persist thousands of years after glacier retreat in a
558 state of disequilibrium with current conditions.

559 **6 Implications**

560 Two primary implications arise from this work. First, the sediment budget presented in Figure 3
561 illustrates the dependence of sediment budget results on the measurement period. Not only will
562 the total budget volumes reflect the specific set of conditions experienced throughout the
563 measurement period, but the overall patterns of erosion and deposition and subsequently the
564 delivery ratios will also vary. During extreme events, thresholds are surpassed, sources of
565 disconnectivity become less effective at trapping and storing sediment (and may even become
566 sources), and the efficiency of sediment transfer increases resulting in rapid adjustment.
567 Sediment budget studies must carefully acknowledge this reality and interpret their results
568 accordingly. More work is needed that links the frequency and magnitude of hydrological and
569 mass movement events to the efficiency of sediment transfer. A better understanding of this link
570 would help define when it is important to consider disconnectivity.

571 Second, we suggest that as long as effective timescales and event magnitudes are properly
572 considered, mapping sources of sediment disconnectivity can provide a clear picture of sediment
573 dynamics and spatially variable patterns of sediment transfer efficiencies. This work highlights
574 the need for a better understanding of the trapping efficiencies of sources of disconnectivity in
575 relation to events of varying magnitude. Among other potential applications, mapping sources of
576 disconnectivity can strengthen and add context when calculating sediment budgets and
577 identifying important sources of sediment or the effective catchment area. Disconnectivity can
578 also help make sense of the spatiotemporal variability of sediment dynamics, especially for
579 transitional systems. Additionally, many sources of disconnectivity can be directly observed and
580 mapped both remotely and in the field, and existing large-scale geomorphic, landform, and
581 terrain classification maps may be reinterpreted in the context of disconnectivity. It is impractical
582 to seek an understanding of catchment-scale sediment dynamics without the explicit
583 consideration of disconnectivity, as it is such a common state of geomorphic systems.

7 Conclusions

In this study, we investigate catchment-scale sediment dynamics through sediment budgeting and mapping sources of disconnectivity. The Tahoma Creek watershed drains the southwest flank of Mount Rainier, Washington, USA, and is incredibly dynamic as a result of impressive topographic relief, large stores of unconsolidated glacial sediment in the headwaters, and retreating glaciers that produce glacial outburst floods and debris flows. In constructing a conceptual and quantitative sediment budget, we found that the proglacial zone supplies up to 80% of the total sediment. Frequent debris flows and floods, and high connectivity within the proglacial zone and upper reaches of Tahoma Creek result in a rapid response to changing conditions (i.e., glacier retreat) and intense geomorphic change. However, down valley, the hillslopes become decoupled from the active channel, sources of disconnectivity become increasingly more abundant, and sediment transfer efficiencies decrease resulting in roughly half of the eroded sediment being redeposited. Sediment storage and disconnectivity increase landscape resilience to change and delay, disperse, and disrupt signal propagation. Sources of sediment disconnectivity may persist for thousands of years controlling the spatial patterns of sediment transfers. For example, glacial macroforms such as parklands, glacial cirques, and breached divides persist relatively unchanged in a state of disequilibrium with modern conditions.

We also found that the spatial distribution of sources of disconnectivity and their upslope affected areas explains the spatial patterns of sediment transfers and assumed transfer efficiencies within the watershed. Mapping sources of disconnectivity provides a straightforward approach to estimating system disconnectivity. Even locations with intense morphodynamics, such as Mount Rainier, are predominantly disconnected over human timescales. We therefore suggest that disconnectivity is the dominant state of natural systems and warrants further research. Integrating sources of disconnectivity within connectivity indices or creating an index of disconnectivity would be an interesting avenue of future work. Investigating disconnectivity over longer time periods may also prove useful for understanding landscape evolution, particularly in the context of glacial cycles.

Acknowledgments

M. Turley was supported by the Department of Geography at the University of British Columbia. Additional funding was provided by a NSERC Discovery Grant (to M. Hassan). Discussions and guidance from Olav Slaymaker motivated and refined this project. This work also benefited from insightful discussions with, and data provided by Scott Anderson. We thank Scott Beason, Taylor Kenyon, and Robby Jost of the U.S. National Park Service at Mount Rainier National Park for assistance with fieldwork preparation and safety planning. We would also like to thank Amy East, and Michéle Koppes for comments on drafts of this work.

Conflict of Interest

The authors declare that they have no conflicts of interest.

Author Contributions

The study design was developed by M. Turley and M. Hassan. Data collection and fieldwork was completed by M. Turley. Data analysis was completed by M. Turley under the supervision of M. Hassan. The initial draft and subsequent revisions of the manuscript were completed by M. Turley and M. Hassan.

Data Availability Statement

Lidar data are openly available through the Washington Department of Natural Resource's lidar portal, available at https://lidarportal.dnr.wa.gov. The specific lidar datasets used are entitled, "Rainier West 2002 - DTM", "Rainier 2007 - DTM", and "Rainier 2012 – DTM". The 2009 NAIP imagery is available through the US Department of Agriculture Geospatial Data Gateway, at "https://datagateway.nrcs.usda.gov/GDGHome_DirectDownLoad.aspx". Sediment budget data can be found at Turley and Hassan (2023, https://doi.org/10.6084/m9.figshare.22045217).

References

Al-Ghorani, N. G., Hassan, M. A., & Langendoen, E. J. (2022). Reach-scale morphodynamics: Insights from 20 years of observations and model simulations. *Geomorphology*, *413*. https://doi.org/10.1016/j.geomorph.2022.108375

Anderson, S. (2013). Sediment fluxes in a changing climate: Tahoma Creek over daily to centennial time-scales (master's *thesis*). University of Colorado at Boulder.

Anderson, S. W., & Konrad, C. P. (2019). Downstream-propagating channel responses to decadal-scale climate variability in a glaciated river basin. *Journal of Geophysical Research: Earth Surface*, 124, 902- 919. https://doi.org/10.1029/2018JF004734

Anderson, S., & Pitlick, J. (2014). Using repeat lidar to estimate sediment transport in a steep stream. *Journal of Geophysical Research: Earth Surface*, 621–643. https://doi.org/10.1002/2013JF002933.Received

651 Anderson, S., & Shean, D. (2021). Spatial and temporal controls on proglacial erosion rates: a
652 comparison of four basins on Mount Rainier, 1960 to 2017. *Earth Surface Processes and*
653 *Landforms*, 1–50. https://doi.org/10.1002/esp.5274

654 Ballantyne, C. K. (2002). Paraglacial Geomorphology. *Quaternary Science Reviews*, *21*, 1935–
655 2017. https://doi.org/10.1016/B978-0-444-53643-3.00089-3

656 Beason, S. (2017). Change in glacial extent at Mount Rainier National Park from 1896 to 2015.
657 Natural Resource Report. NPS/MORA/NRR-2017/1472, 98.
658 http://www.morageology.com/pubs/12.pdf

659 Beason, S. R., Legg, N. T., Kenyon, T. R., Jost, R. P., & Kennard, P. M. (2019). Forecasting and
660 seismic detection of debris flows in pro-glacial rivers at Mount Rainier National Park,
661 Washington, USA. *7th International Conference on Debris-Flow Hazards Mitigation*.

662 Benda, L., Andras, K., Miller, D., & Bigelow, P. (2004). Confluence effects in rivers:
663 Interactions of basin scale, network geometry, and disturbance regimes. *Water Resources*
664 *Research*, *40*, 1–15. https://doi.org/10.1029/2003WR002583

665 Ben-Israel, M., Armon, M., & Matmon, A. (2022). Sediment residence times in large rivers
666 quantified using a cosmogenic nuclides based transport model and implications for buffering of
667 continental erosion signals. *Journal of Geophysical Research: Earth Surface*, *127*(5).
668 https://doi.org/10.1029/2021JF006417

669 Brardinoni, F., & Hassan, M. A. (2006). Glacial erosion, evolution of river long profiles, and the
670 organization of process domains in mountain drainage basins of coastal British Columbia.
671 *Journal of Geophysical Research*, *111*(F1), F01013. https://doi.org/10.1029/2005JF000358

672 Cavalli, M., Trevisani, S., Comiti, F., & Marchi, L. (2013). Geomorphometric assessment of
673 spatial sediment connectivity in small Alpine catchments. *Geomorphology*, *188*, 31–41.
674 https://doi.org/10.1016/j.geomorph.2012.05.007

675 Carrivick, J. L., & Heckmann, T. (2017). Short-term geomorphological evolution of proglacial
676 systems. *Geomorphology*, *287*, 3–28. https://doi.org/10.1016/j.geomorph.2017.01.037

677 Chorley, R.J., Kennedy, B.A. (1971). Physical geography: A systems approach. *Prentice-Hall*
678 *International*, London. 370 pp.

679 Church, M., & Slaymaker, O. (1989). Disequilibrium of Holocene sediment yield in glaciated
680 British Columbia. *Nature*, *337*(6206), 452–454. https://doi.org/10.1038/337452a0

681 Church, M., & Ryder, J. M. (1972). Paraglacial sedimentation: A consideration of fluvial
682 processes conditioned by glaciation. *Geological Society of America Bulletin*, *83*, 3059–3072.

683 Cienciala, P. (2021), Vegetation and geomorphic connectivity in mountain fluvial systems.
684 *Water*, 13, 593. https://doi.org/10.3390/w13050593

685 Cienciala, P., & Hassan, M. A. (2013). Linking spatial patterns of bed surface texture, bed
686 mobility, and channel hydraulics in a mountain stream to potential spawning substrate for small
687 resident trout. *Geomorphology*, *197*, 96–107. https://doi.org/10.1016/j.geomorph.2013.04.041

688 Cossart, E. (2008). Landform connectivity and waves of negative feed- backs during the
689 paraglacial period, a case study: The Tabuc sub-catchment since the end of the Little Ice Age

(Massif des Ecrins, France). *Géomorphologie: Relief, Processus, Environnement*, 14(4), 249–260.

Cossart, É., & Fressard, M. (2017). Assessment of structural sediment connectivity within catchments: insights from graph theory. *Earth Surface Dynamics*, *5*, 253–268. https://doi.org/10.5194/esurf-5-253-2017

Crandell, D. R. (1971). Postglacial lahars from Mount Rainier Volcano, Washington. *U. S. Geological Survey Professional Paper*, *667*, 80.

Crandell, D. R., & Miller, R. D. (1974). Quaternary stratigraphy and extent of glaciation in the Mount Rainier region, Washington. *U. S. Geological Survey Professional Paper*, 59.

Curry, A. M., Sands, T. B., & Porter, P. R. (2009). Geotechnical controls on a steep lateral moraine undergoing paraglacial slope adjustment. *Geological Society, London, Special Publications*, *320*(1), 181–197. https://doi.org/10.1144/SP320.12

Dietrich, W. E., Dunne, T., Humphrey, N. F., & Reid, L. M. (1982). Construction of sediment budgets for drainage basins. In F. J. Swanson, R. J. Janda, Thomas Dunne, & D. N. Swanston (Eds.), *Sediment budgets and routing in forested drainage basins* (pp. 5–23). Pacific Northwest Forest and Range Experiment Station, General Technical Report PNW-141.

East, A. E., & Sankey, J. B. (2020). Geomorphic and sedimentary effects of modern climate change: Current and anticipated future conditions in the western United States. *Reviews of Geophysics*, 58, e2019RG000692. https://doi.org/10.1029/2019RG000692

Eaton, B. C., MacKenzie, L. G., & Booker, W. H. (2020). Channel stability in steep gravel–cobble streams is controlled by the coarse tail of the bed material distribution. *Earth Surface Processes and Landforms*, *45*(14), 3639–3652. https://doi.org/10.1002/esp.4994

Fahnestock, R. K. (1963). Morphology and hydrology of a glacial stream - White River, Mount Rainier Washington. *Geological Survey Professional Paper*, *422-A*, 1–70.

Fiske, R. S., Hopson, C. A., & Waters, A. C. (1963). Geology of Mount Rainier National Park, Washington. *Geological Survey Professional Paper*, *444*.

Fressard, M. & Cossart, E. (2019). A graph theory tool for assessing structural sediment connectivity: Development and application in the Mercurey vineyards (France). *Science of the Total Environment*, *651*, 2566–2584. https://doi.org/10.1016/j.scitotenv. 2018.10.158

Fryirs, K. A., Brierley, G. J., Preston, N. J., & Kasai, M. (2007a). Buffers, barriers and blankets: The (dis)connectivity of catchment-scale sediment cascades. *Catena*, *70*(1), 49–67. https://doi.org/10.1016/j.catena.2006.07.007

Fryirs, K. A., Brierley, G. J., Preston, N. J., & Spencer, J. (2007b). Catchment-scale (dis)connectivity in sediment flux in the upper Hunter catchment, New South Wales, Australia. *Geomorphology*, *84*(3–4), 297–316. https://doi.org/10.1016/j.geomorph.2006.01.044

Fryirs, K. A. (2013). (Dis)Connectivity in catchment sediment cascades: A fresh look at the sediment delivery problem. *Earth Surface Processes and Landforms*, *38*(1), 30–46. https://doi.org/10.1002/esp.3242

Fryirs, K. A. (2017). River sensitivity: a lost foundation concept in fluvial geomorphology. *Earth Surface Processes and Landforms*, *42*(1), 55–70. https://doi.org/10.1002/esp.3940

730 Gran, K. B., & Czuba, J. A. (2017). Sediment pulse evolution and the role of network structure.
731 *Geomorphology*, *277*, 17–30. https://doi.org/10.1016/j.geomorph.2015.12.015

732 Grant, G. E., O'Connor, J., & Safran, E. (2017). Excursions in fluvial (dis)continuity.
733 *Geomorphology*, *277*, 145–153. https://doi.org/10.1016/j.geomorph.2016.08.033

734 Harvey, A. M. (2002). Effective timescales of coupling within fluvial systems. *Geomorphology*,
735 *44*(3–4), 175–201. https://doi.org/10.1016/S0169-555X(01)00174-X

736 Hassan, M. A., Bird, S., Reid, D. A., Ferrer-Boix, C., Hogan, D., Brardinoni, F., & Chartrand, S.
737 M. (2018). Variable hillslope-channel coupling and channel characteristics of forested mountain
738 streams in glaciated landscapes. *Earth Surface Processes and Landforms*, 16.
739 https://doi.org/10.1002/esp.4527

740 Heckmann, T. & Vericat, D. (2018). Computing spatially distributed sediment delivery ratios:
741 inferring functional sediment connectivity from repeat high-resolution digital elevation models.
742 *Earth Surface Processes and Landforms*, *43*(7), 1547–1554. https://doi.org/10.1002/ esp.4334

743 Hinderer, M. (2012). From gullies to mountain belts: A review of sediment budgets at various
744 scales. *Sedimentary Geology*, *280*, 21–59. https://doi.org/10.1016/j.sedgeo.2012.03.009

745 Hoffmann, T., Müller, T., Johnson, E., & Martin, Y. (2013). Postglacial adjustment of steep,
746 low-order drainage basins, Canadian Rocky Mountains. *Journal of Geophysical Research: Earth*
747 *Surface*, 118. doi:10.1002/2013JF002846.

748 Hoffmann, T. (2015). Sediment residence time and connectivity in non-equilibrium and transient
749 geomorphic systems. *Earth-Science Reviews*, *150*, 609–627.
750 https://doi.org/10.1016/j.earscirev.2015.07.008

751 Hooke, J. M. (2003). Coarse sediment connectivity in river channel systems: A conceptual
752 framework and methodology. *Geomorphology*, *56*(1–2), 79–94. https://doi.org/10.1016/S0169-
753 555X(03)00047-3

754 Lane, S. N., Bakker, M., Gabbud, C., Micheletti, N., & Saugy, J.-N. (2017). Sediment export,
755 transient landscape response and catchment-scale connectivity following rapid climate warming
756 and Alpine glacier recession. *Geomorphology*, *277*, 210–227.
757 https://doi.org/10.1016/j.geomorph.2016.02.015

758 Leenman, A., & Tunnicliffe, J. F. (2020). Tributary-junction fans as buffers in the sediment
759 cascade: a multi-decadal study. *Earth Surface Processes and Landforms*, *45*(2), 265–279.
760 https://doi.org/10.1002/esp.4717

761 Legg, N. T., Meigs, A. J., Grant, G. E., & Kennard, P. (2014). Debris flow initiation in proglacial
762 gullies on Mount Rainier, Washington. *Geomorphology*, *226*, 249–260.
763 https://doi.org/10.1016/j.geomorph.2014.08.003

764 Lisenby, P. E., Fryirs, K. A., & Thompson, C. J. (2020). River sensitivity and sediment
765 connectivity as tools for assessing future geomorphic channel behavior. *International Journal of*
766 *River Basin Management*, *18*(3), 279–293. https://doi.org/10.1080/15715124.2019.1672705

767 Micheletti, N., & Lane, S. N. (2016). Water yield and sediment export in small, partially
768 glaciated Alpine watersheds in a warming climate. *Water Resources Research*, *52*(51), 5974–
769 5997. https://doi.org/10.1002/2016WR018977

Najafi, S., Dragovich, D., Heckmann, T., & Sadeghi, S. H. (2021). Sediment connectivity concepts and approaches. *Catena*, *196*, 104880. https://doi.org/10.1016/j.catena.2020.104880

Nicholas, A. P., Ashworth, P. J., Kirkby, M. J., Macklin, M. G., & Murray, T. (1995). Sediment slugs: Large-scale fluctuations in fluvial sediment transport rates and storage volumes. *Progress in Physical Geography*, *19*(4), 500–519. https://doi.org/10.1177/030913339501900404

Ortíz-Rodríguez, A.J., Borselli, L. & Sarocchi, D. (2017). Flow connectivity in active volcanic areas: Use of index of connectivity in the assessment of lateral flow contribution to main streams. *Catena*, 157(October), 90–111. https://doi.org/10.1016/j.catena.2017.05.009

Reid, L.M. & Dunne, T. (1996). Rapid evaluation of sediment budgets. *GeoEcology Paperbacks*, Catena Verlag, Germany.

Reid, L.M. & Dunne, T. (2016). Sediment budgets as an organizing framework in fluvial geomorphology. In *Tools in Fluvial Geomorphology* (eds G.M. Kondolf and H. Piégay). https://doi.org/10.1002/9781118648551.ch16

Reid, D. A., Hassan, M. A., & McCleary, R. J. (2021). Glacial landscape configuration influences channel response to flooding. *Earth Surface Processes and Landforms*. https://doi.org/10.1002/esp.5240

Repasch, M., Wittmann, H., Scheingross, J. S., Sachse, D., Szupiany, R., Orfeo, O., Fuchs, M., & Hovius, N. (2020). Sediment transit time and floodplain storage dynamics in alluvial rivers revealed by meteoric 10Be. *Journal of Geophysical Research: Earth Surface*, *125*(7), 1–19. https://doi.org/10.1029/2019JF005419

Richardson, D. (1968). Glacier outburst floods in the Pacific Northwest. *U. S. Geological Survey Professional Paper*, *600-D*, D79–D86.

Riedel, J., & Dorsch, S. (2016). Geomorphology of Mount Rainier landform mapping at Mount Rainier National Park, Washington. *Natural Resource Report*, *1234*.

Schumm, S. A. (1979). Geomorphic thresholds: the concept and its applications. *Transactions of the Institute of British Geographers*, 485–515.

Scott, D. N., & Collins, B. D. (2021). Frequent mass movements from glacial and lahar terraces, controlled by both hillslope characteristics and fluvial erosion, are an important sediment source to Puget Sound rivers. *Water Resources Research*. https://doi.org/10.1029/2020wr028389

Scott, K. M., Vallance, J. W., & Pringle, P. T. (1995). Sedimentology, behavior, and hazards of debris flows at Mount Rainier, Washington. *Geological Survey Professional Paper*, *1547*.

Sigafoos, R. S., & Hendricks, E. L. (1972). Recent activity of glaciers of Mount Rainier, Washington. *Geological Survey Professional Paper*, *387-B*.

Slaymaker, O. (2004). Mass balances of sediments, solutes and nutrients: The need for greater integration. *Journal of Coastal Research*, *SPEC. ISS. 43*, 109–123.

Slaymaker, O., & Embleton-Hamann, C. (2018). Advances in global mountain geomorphology. *Geomorphology*, *308*, 230–264. https://doi.org/10.1016/j.geomorph.2018.02.016

Tofelde, S., Bernhardt, A., Guerit, L., & Romans, B. W. (2021). Times associated with source-to-sink propagation of environmental signals during landscape transience. *Frontiers in Earth Science*, *9*, *1–26*. https://doi.org/10.3389/feart.2021.62831

Turley, M., & Hassan, M. A. (2023). Datasets for quantitative sediment budget analysis: Tahoma Creek Watershed, WA, USA. [dataset]. https://doi.org/10.6084/m9.figshare.22045217

Turley, M., Hassan, M. A., & Slaymaker, O. (2021). Quantifying sediment connectivity: Moving toward a holistic assessment through a mixed methods approach. *Earth Surface Processes and Landforms*, *46*(12), 2501–2519. https://doi.org/10.1002/esp.5191

US Department of Agriculture. (2019). Geospatial data gateway. Available at: http://datagateway.nrcs.usda.gov. Accessed February 2019.

Walder, J. S., & Driedger, C. L. (1994a). Rapid geomorphic change caused by glacial outburst floods and debris flows along Tahoma Creek, Mount Rainier, Washington, U.S.A. *Arctic and Alpine Research*, *26*(4), 319–327.

Walder, J. S., & Driedger, C. L. (1994b). Geomorphic change caused by outburst floods and debris flows at Mount Rainier, Washington, with emphasis on Tahoma Creek Valley. *Water-Resources Investigations Report, 93–4093*.

Walling, D. E. (1983). The sediment delivery problem. *Journal of Hydrology*, *65*, 209–237.

Whiting, P.J. & Bradley, J.B. (1993) A process-based classification system for headwater streams. *Earth Surface Processes and Landforms*, *18*(7), 603–612. https://doi.org/10.1002/esp.3290180704

Wohl, E. E., Brierley, G. J., Cadol, D., Coulthard, T. J., Covino, T., Fryirs, K. A., Grant, G. E., Hilton, R. G., Lane, S. N., Magilligan, F. J., Meitzen, K. M., Passalacqua, P., Poeppl, R. E., Rathburn, S. L., & Sklar, L. S. (2019). Connectivity as an emergent property of geomorphic systems. *Earth Surface Processes and Landforms*. https://doi.org/10.1002/esp.4434